Accepted Manuscript

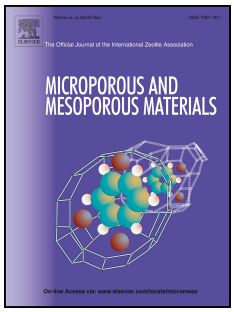

Controlled Delivery of Drugs Adsorbed onto porous Fe_3O_4 Structures by Application of AC/DC Magnetic Fields

Mislav Mustapić, Md Shahriar Al Hossain, Joseph Horvat, Pawel Wagner, David R.G. Mitchell, Jung Ho Kim, Gursel Alici, Yoshitaka Nakayama, Boris Martinac

PII: S1387-1811(15)00696-4

DOI: 10.1016/j.micromeso.2015.12.032

Reference: MICMAT 7469

To appear in: *Microporous and Mesoporous Materials*

Received Date: 7 August 2015

Revised Date: 27 November 2015

Accepted Date: 14 December 2015

Please cite this article as: M. Mustapić, M.S. Al Hossain, J. Horvat, P. Wagner, D.R.G. Mitchell, J.H. Kim, G. Alici, Y. Nakayama, B. Martinac, Controlled Delivery of Drugs Adsorbed onto porous Fe_3O_4 Structures by Application of AC/DC Magnetic Fields, *Microporous and Mesoporous Materials* (2016), doi: 10.1016/j.micromeso.2015.12.032.

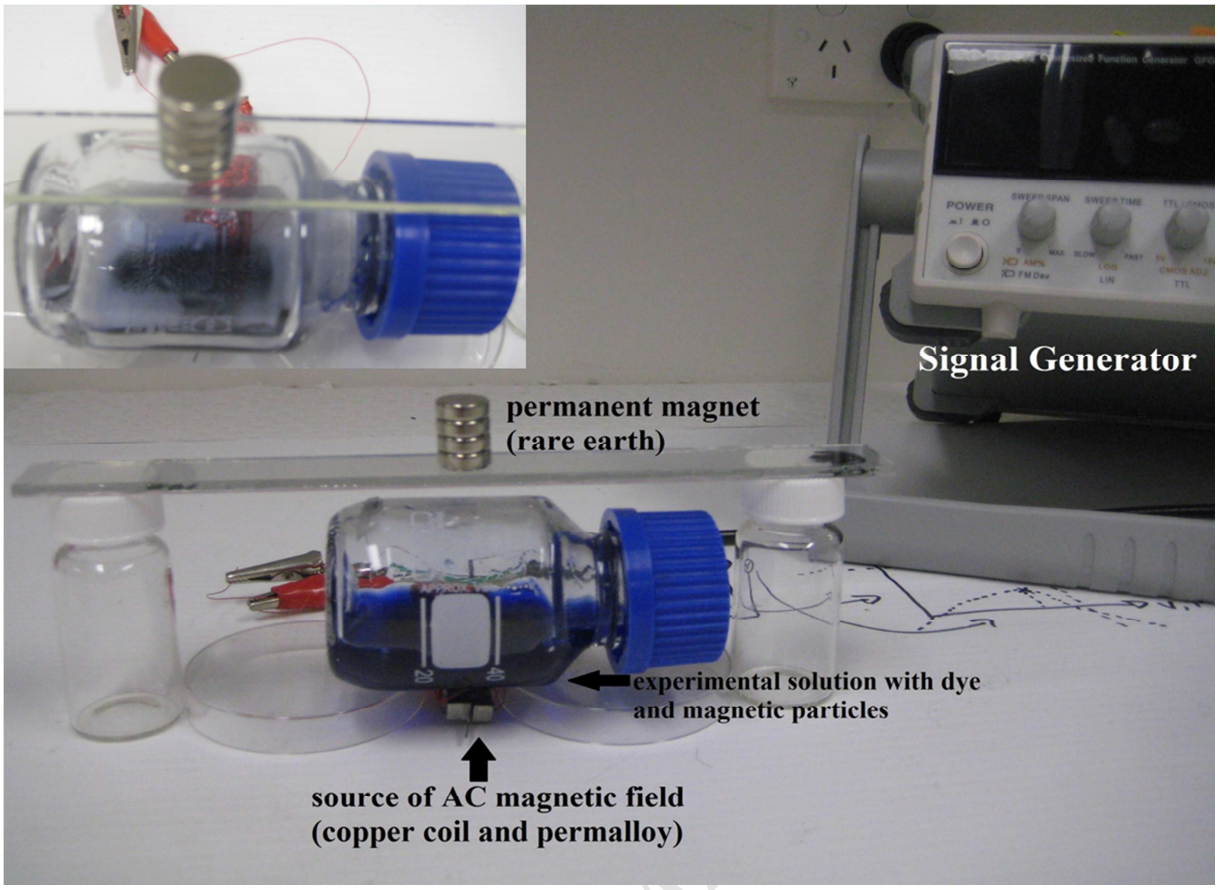

Experimental apparatus of simple and highly efficent set up showing how AC and DC magnetic fields were applied. Combination of AC/DC magnetic fields provide maximal release of methil blue dye.

Controlled Delivery of Drugs Adsorbed onto porous Fe_3O_4 Structures by Application of AC/DC Magnetic Fields

Mislav Mustapić[1,7*], Md Shahriar Al Hossain[1*], Joseph Horvat[1], Pawel Wagner[2], David R. G. Mitchell[3], Jung Ho Kim[1], Gursel Alici[4], Yoshitaka Nakayama[5], Boris Martinac[5,6]

[1]Institute for Superconducting and Electronic Material (ISEM), University of Wollongong, Squires Way, North Wollongong NSW 2522,
[2]Intelligent Polymer Research Institute/AIIM Faculty Innovation Campus, Squires Way, University of Wollongong NSW 2522,
[3]Electron Microscopy Centre/AIIM Faculty Innovation Campus, Squires Way, University of Wollongong NSW 2522,
[4]School of Mechanical, Materials and Mechatronic Engineering and ARC Centre of Excellence for Electromaterials Science , University of Wollongong, NSW, 2522, Australia
[5]Molecular Cardiology and Biophysics Division, Victor Chang Cardiac Research Institute, NSW 2010, Australia,
[6]St Vincent's Clinical School, University of New South Wales, Darlinghurst, NSW 2010
[7]University of Osijek, Department of Physics, Osijek, Croatia.

*Corresponding authors:
e-mail address: mislav.mustapic@gmail.com, shahriar@uow.edu.au
Phone: +385 976336964

Abstract:

Porous structures made up of Fe_3O_4 nanoparticles were used to adsorb methyl blue in water. Controlled release of the methyl blue to water was then achieved by application of a magnetic field. Application of a pure DC field did not result in any release. Application of a pure AC field caused released of the methyl blue. However, a combination of both DC and AC fields resulted in much faster release. The mechanism by which this operated is believed to result from viscous friction. Nanoparticles are strongly aligned in the DC field and oscillate under the influence of the AC field. This study demonstrates a concept for controlled drug delivery, where pharmaceutical molecules, similar to methyl blue, would be adsorbed onto porous Fe_3O_4 structure and the released at a target by application of appropriately localised magnetic fields.

1. Introduction:

Design and construction of a complete drug delivery system, from a drug nano-carrier to an efficient system for drug activation in a localised volume of the human body requires a multidisciplinary approach and substantial investment. Selection of proper drug-carriers from various candidates such as liposomes [1,2,3], nanoparticles, porous materials [4,5,6,7,8], polymer-drug conjugates [9,10,11], protein (albumin) nanoparticles [12,13,14], polymeric micelles [15,16,17], is the first part of this effort. Porous materials possess a large surface area and so have the capability to store different molecules (drugs) within this structure making them potential drug carriers.

In this paper we demonstrate that porous Fe_3O_4 structures can be used as a vehicle for the transport of drugs adsorbed onto their porous surface. This material enables controlled release of the chemical payload via activation by a magnetic field. We used methyl blue as a surrogate drug. It adsorbs onto the Fe_3O_4 surface, and its release into the surrounding water via application of a magnetic field that can be monitored quite readily by measuring the light absorption through water. This is a proof of the concept that organic molecules can be adsorbed onto an Fe_3O_4 carrier and the release thereof controlled by an external stimulus (applied magnetic field).

Methyl blue is a common biological dye, as is methylene blue, one of the first synthetic drugs. These dyes attach to the tissues through electrostatic interaction. We believe the same mechanism is responsible for the loading of methyl blue onto our porous Fe_3O_4 structures. Drugs that are electrically charged when dissolved in water are likely candidates for loading into the Fe_3O_4 structures.

Furthermore, a great advantage of Fe_3O_4 nanoparticles is their biological compatibility [18,19,20]. Such an important feature enables the use of the nanoparticles without a

requirement for biologically tolerable coatings, which might otherwise degrade their saturation magnetization and drug absorption ability.

2. Methods and experiments:

2.1 Synthesis of Fe_3O_4 nanoparticles

Magnetite nanoparticles were synthesised with a wet technique by forming a micro-emulsion solution, similar to that used in our previous work [21,19]. Iron sources used were iron (II) chloride and iron (III) chloride dissolved in deionised (DI) water in separate beakers in a molar ratio of 1:2. The solution with iron (II) ions was maintained under an argon atmosphere to eliminate oxidation to iron (III). Both solutions were stirred for half an hour. The micro-emulsion Me1 was prepared in the third beaker.

The micro-emulsion Me1 used in this research consisted of cyclohexane (organic solvent), cationic surfactant hexadecyltrimethylammoniumbromide (CTAB), and anionic surfactant sodium dodecyl sulfate (SDS). A combination of two different polarity types of surfactants is required because of the possible formation of larger vacancies inside Fe_3O_4 samples (attraction between them), as well as creation of bilayer vesicles.

In the next step the micro-emulsion Me1 and solution of Fe^{3+} were added to a solution of Fe^{2+} maintained in argon to form the micro-emulsion Me2. Shortly after that, 30w% ammonium solution was added from a separation funnel to Me2. The formation of black particles started immediately upon adding the ammonium solution.

Black powders were collected and washed several times with DI water and acetone and dried overnight. Next day the dried black powders were heated in a furnace at 250°C for 2 hours in a protective argon atmosphere.

2.2 Structural characterization

TEM imaging was performed using a probe-corrected JEOL ARM200F equipped with a cold field emission gun and a Gatan UltraScan CCD. The microscope was also equipped with a JEOL large area EDS detector with collection angle of ~1 sr. The black powder sample was suspended in an emulsion of water and cyclohexane, centrifuged, and drop-cast on a Holey carbon Cu grid for TEM/STEM observation. All imaging and analysis was carried out using 200kV electrons.

X-ray powder diffraction (XRD) was carried out on a Philips diffractometer, model PW1820 (Cu K_α radiation), in Bragg–Brentano geometry.

ASAP2000 (Micromeritics, USA) gas sorption analyser was used to determine the adsorption/desorption isotherm, specific surface area and pore size distribution of the sample. Pre-weighed powders were degassed at 300°C to a residual pressure of 6.67 Pa. Analysis was then performed using N_2 as the adsorbate at 77K.

2.3 Magnetic measurement

Magnetic measurements on nanoparticles were performed using a Quantum Design MPMS-5T SQUID magnetometer. Magnetic hysteresis loops M(H) were measured in an applied field within a range of 2T at three different temperatures (10K, 100K, and 310K) temperatures.

2.4 Cytotoxicity test of the Fe_3O_4

The cultures of A549 human lung cancer cells and trypan blue stain have been used in cytotoxicity experiments. Detailed description of cytotoxicity experiments has been reported in our previous work. Similar to our previous work with $CoFe_2O_4$ nanoparticles [21], the cells from all the cultures with porous Fe_3O_4 exhibited negligible cytotoxicity with cell viability ranging close to the blank culture, as can be seen in Fig. 3b.

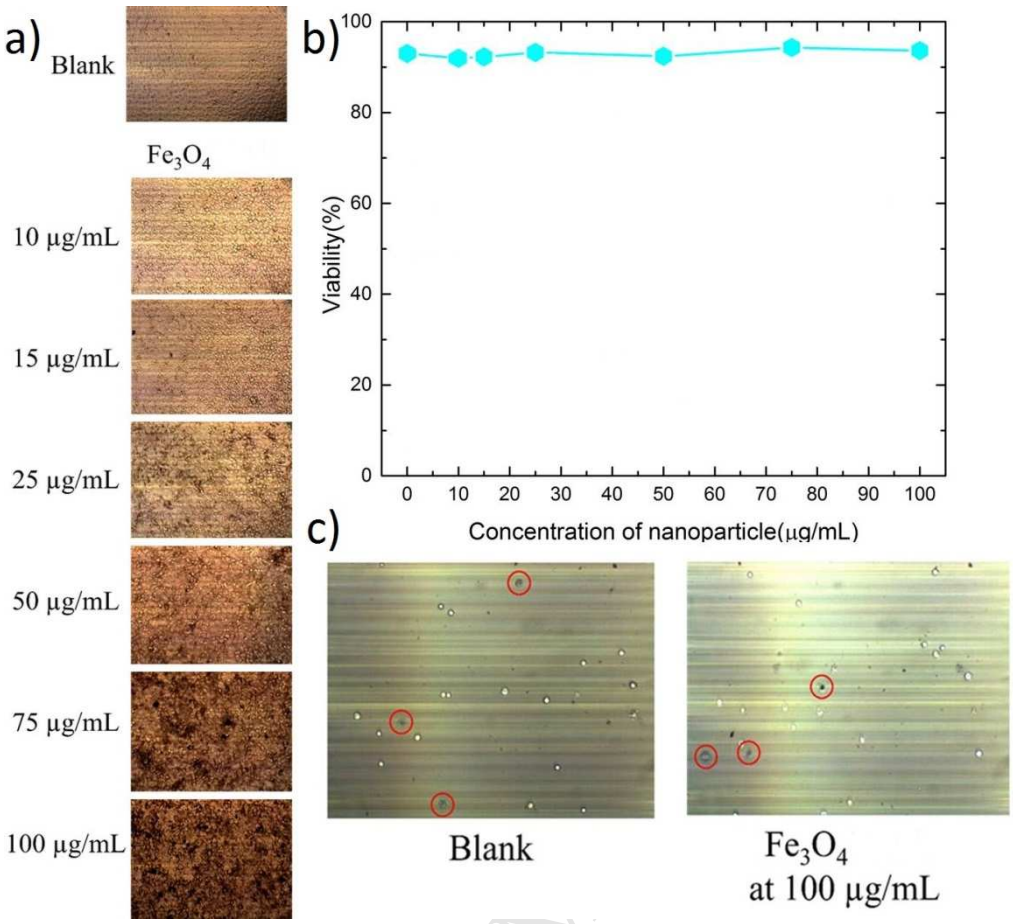

Figure 1.: Cytotoxicity of the Fe_3O_4 sample. *a)* Images of cells in culture with an increasing concentration of the Fe_3O_4; *b)* cell viability in different concentrations of the nanoparticles; *c)* cells after staining with trypan blue showing uncoloured alive cells and blue dead cells.

2.5 AC/DC magnetic field testing:

The experimental testing system was made from simple components as shown in Fig. 1. A commercial permanent magnet (rare earth) was placed on the top of the setup. A bottle containing porous magnetic particles and methyl blue dye was dispersed in a water solution. The AC magnet made from 750 turns of copper wire wrapped on a permalloy core. This was positioned below the bottle. The copper coil was plugged in a signal generator GFG-2000/2100 delivering alternating current of up to 100 mA. The distance between the two magnets (Nd-Fe-B and AC) was 7 cm.

Magnetic Fe_3O_4 nanoparticles were soaked in 0.001 *M* solution of methylene blue (MB) and left overnight to saturate. The nanoparticles were separated from MB solution using permanent magnet and washed several times with DI water. This removed any loosely bound MB, but retained MB within the pores, prior to the application of the magnetic field.

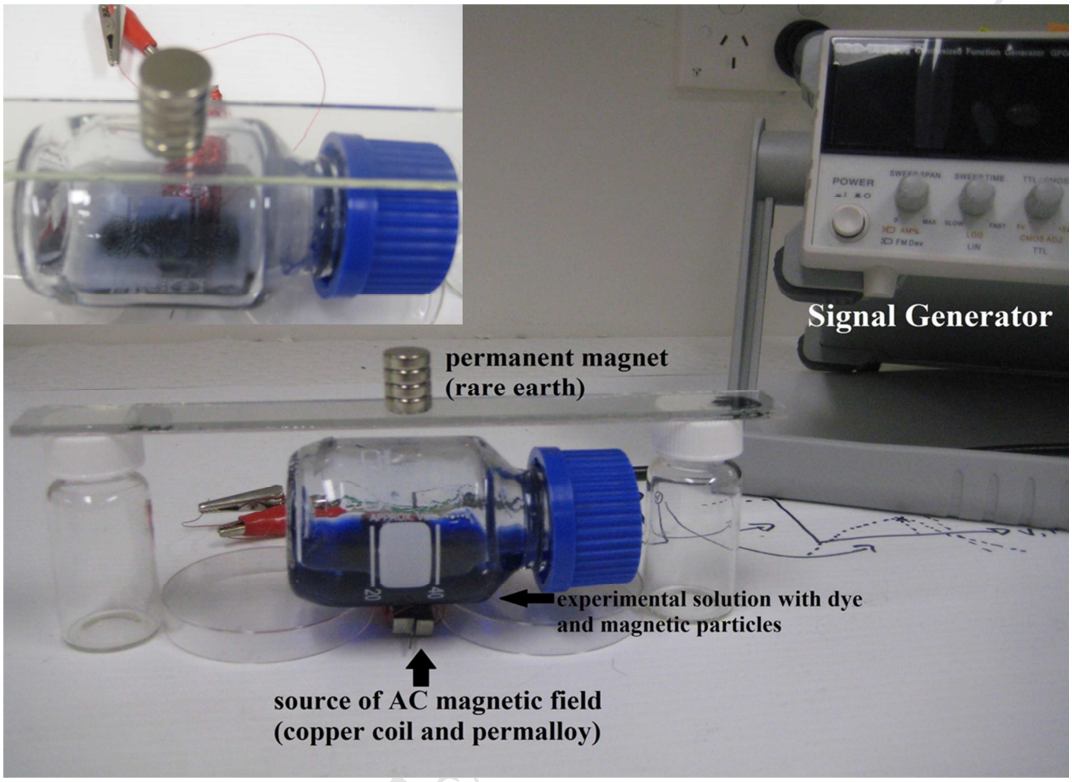

Figure 2.: Experimental apparatus showing how AC and DC magnetic fields were applied.

3. Results and Discussion:

3.1 SEM and TEM analysis:

Imaging and diffraction were carried out in conventional TEM mode. Scanning TEM (STEM) was also used, imaging in high angle annular dark field (HAADF), bright field and secondary electron modes. Figure 2(a,b) are STEM secondary electron images which show agglomeration of roughly spherical particles with particle diameters in the range 10 – 30 nm. SEM secondary electron imaging (Figure 2c,d) showed micron-sized agglomerates with a porosity at the 100nm scale. The agglomerates show extensive porosity, ranging pores from

100nm down to interparticle porosity at less than the particle diameter. To understand this fine scale porosity, TEM was used.

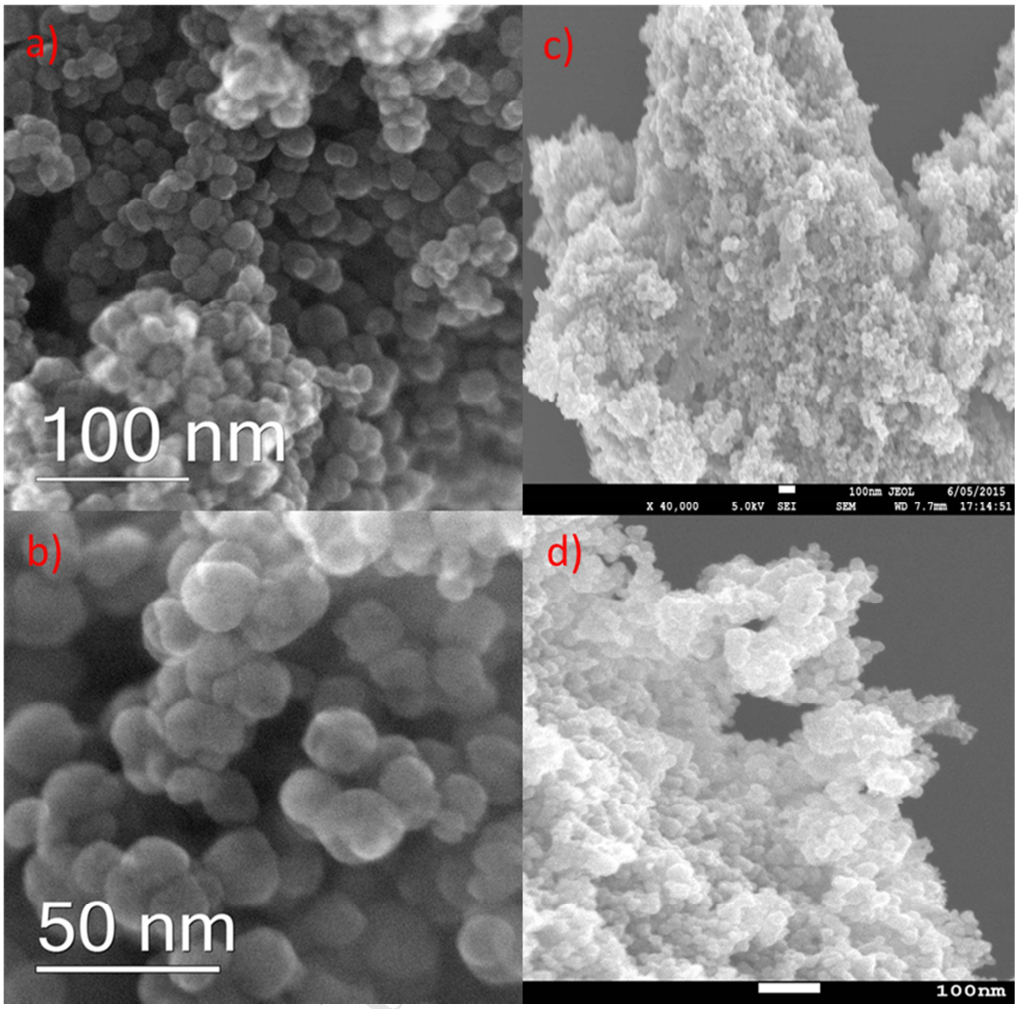

Figure 3.: Secondary electron (SE) images of Fe_3O_4 nanoparticles: *a)* STEM SE image of the surface of an agglomerate composed of 10-30 nm diameter particles; *b)* Detail of a) showing the smooth, rounded particles with extensive open porosity; *c)* and *d)* SEM images showing porosity at up to 100 nm.

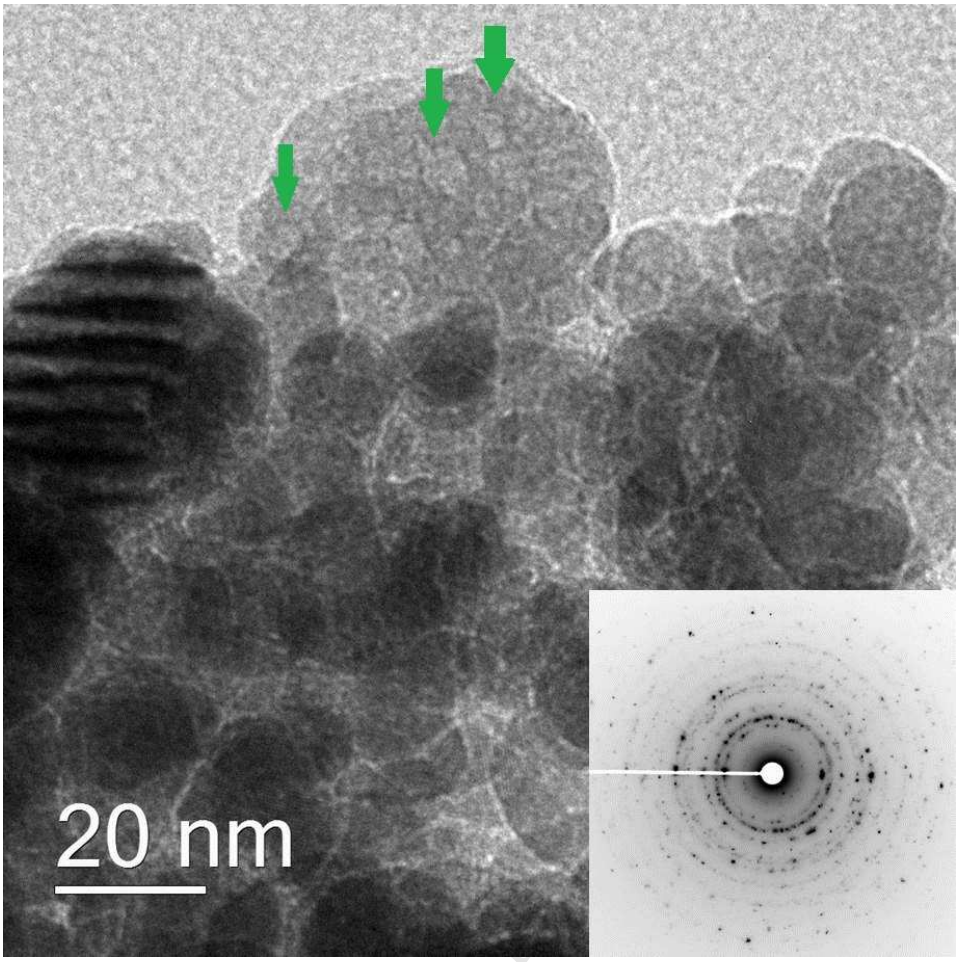

Figure 4.: Bright field TEM image showing crystalline particles 10-50 nm in diameter. Extensive 2-5nm diameter porosity is evident within the larger particles (green arrows). The electron diffraction pattern (inset) shows spacings consistent with magnetite Fe_3O_4.

The TEM images show internal porosity within individual crystallites. Such porosity often forms when low temperature (often amorphous or poorly crystalline) phases densify during heat treatment or crystallisation at higher temperature [22]. The pores are 3-5nm in diameter and show strong faceting. Typically, the internal surfaces of voids are bounded by the densest (low index) planes, such as {100}, {110} and {111} in order to minimise surface energy. This is also true for the external facets of the crystal. The faceting will depend on the crystal structure. The vast majority of these voids are completely internal, since the SE images (Figures 2a, b) do not show any cratering or puckering, where such voids intersect the surface. In fact, during heat treatment the external surface would reconstruct to minimise the

additional surface area induced by a surface-breaking voids. Internal porosity will be fully closed and will not be accessible to MB impregnation and porosimetry measurements.

The inset diffraction pattern in Fig. 3 shows the material to be strongly crystalline. The spotty rings reflect the large number of randomly oriented particles within the field of view from which this pattern was obtained. The pattern contained large bright reflections and more diffuse weak reflections (of similar spacing). The former originated from the largest crystallites (ca 50nm in diameter), while the latter arose from the very smallest crystals (ca10nm). The d-spacings obtained from the pattern showed these results: 0.490, 0.300, 0.257, 0.215, 0.175, 0.164, 0.150, 0.131, 0.122, 0.111, 0.108, 0.100 nm, and they are in good agreement with XRD measurements (JCPDS data for magnetite - below).

3.2 Porosimetry analysis

Specific surface areas were calculated using Brunauer-Emmet-Teller (BET) model [23] from a linear part of BET plot. The value obtained for the Fe_3O_4 porous particles was 11.22 m^2/g. Pore size distribution was calculated from the adsorption branch of isotherm by using Barret-Joyner-Halenda (BJH) model [24]. According to our calculations the pore size distribution is in a range between 5 and 150 nm, with the vast majority ranging between 10 and 50 nm (average pore diameter 10,7 nm.), which is in good agreement with the SEM results.

Considering all specified data we can conclude that examined Fe_3O_4 samples according to IUPAC classification can be characterised as a macro-porous material. Pores smaller than 2 nm have not been observed in porosimetry analysis.

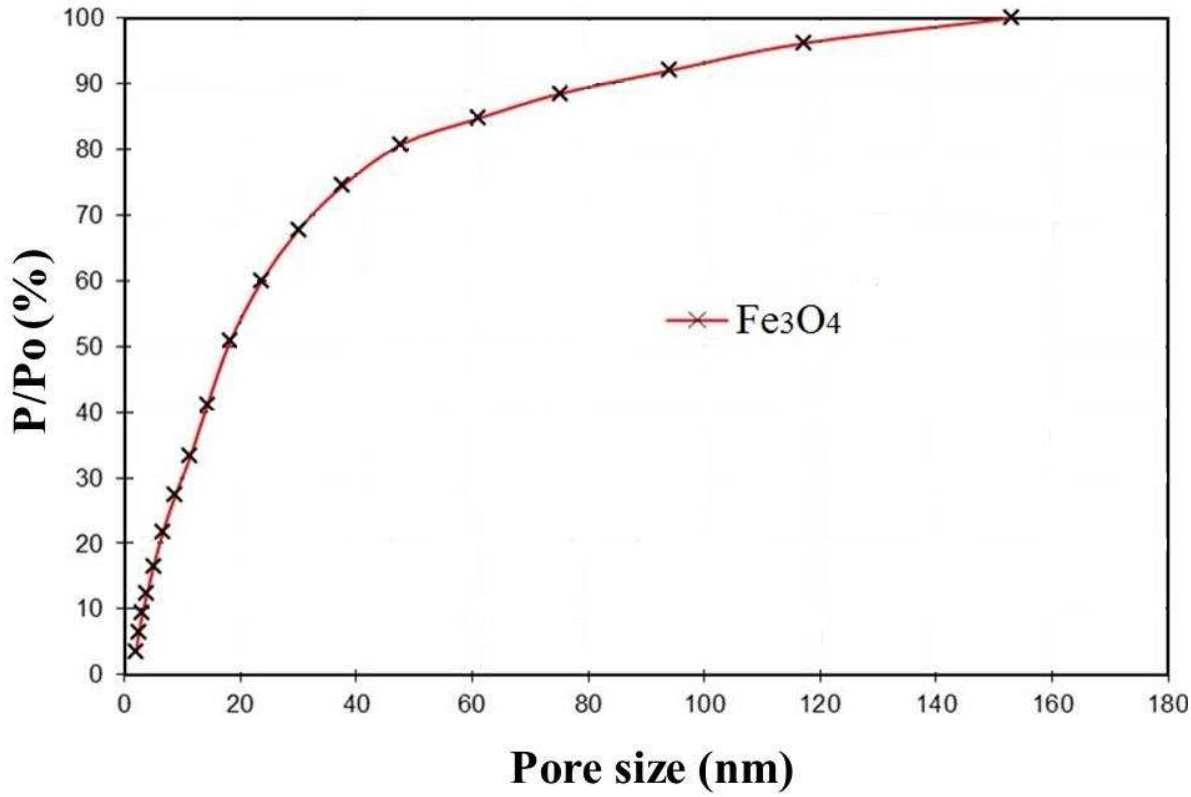

Figure 5.: Capillary hysteresis of nitrogen in pores of Fe_3O_4 at 77 K.

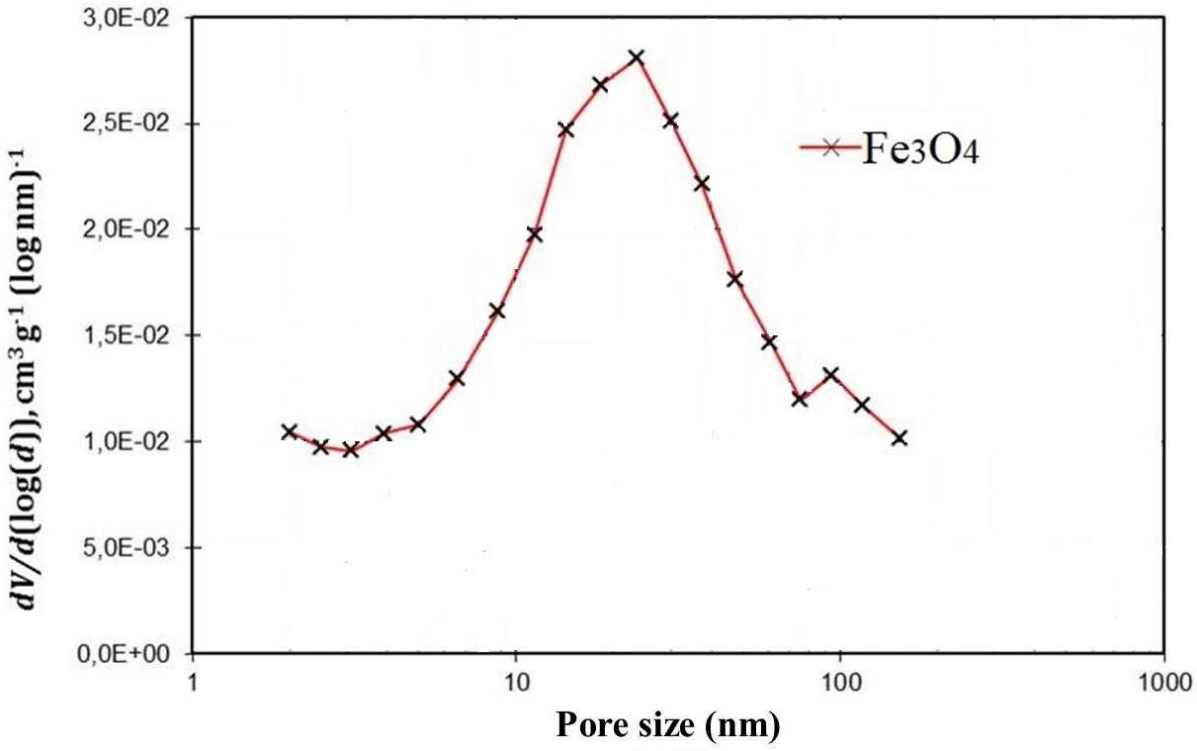

Figure 6.: The pore size distributions of Fe_3O_4 calculated from adsorption-desorption branches of nitrogen isotherms.

3.3 XRD analysis:

X-ray diffraction (XRD) pattern of porous Fe_3O_4 is presented in Figure 4. All indexed peaks belong to the spinel structure of magnetite. A good match was obtained with the standard XRD pattern for magnetite (JCPDS, File No. 00-002-1054), and no other phases were detected. Sharp peaks indicate high crystallinity of the sample in good agreement with the TEM analysis.

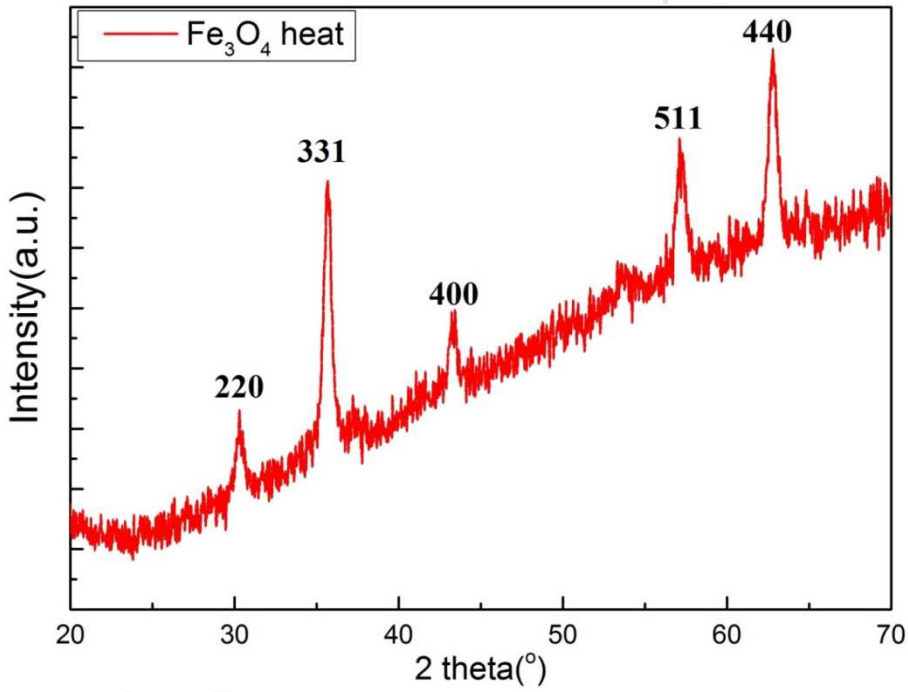

Figure 7.: XRD pattern of porous Fe_3O_4.

3.4 Magnetic measurements:

Figure 5 presents the magnetic hysteresis loops of porous Fe_3O_4 at three different temperatures. The S-shaped hysteresis loops with negligible coercive field (H_C) are a typical feature of superparamagnetic nanoparticles and the results are similar to our previous work on Fe_3O_4 nanoparticles [21,19,25,26]. Application of a magnetic field aligns the magnetic

moments of the nanoparticles and the magnetization of the sample was almost completely saturated at less than 5000 Oe.

The saturation moment (M_s) measured at 10K is quite high and has a value of 85.5 emu g^{-1}, while at 310K the saturation moment was slightly smaller at around 77 emu g^{-1}. These values are comparable to bulk Fe_3O_4, with M_S of 92 emu g^{-1} at T = 10 K [29]. S-shaped magnetic hysteresis loops and small coercive fields were also obtained for nanoparticle Fe_3O_4 reported elsewhere [27,28,29,30], despite the much greater particle size in porous samples prepared here.

The lower M_S of nanoparticles, as compared to larger crystals, occurred because magnetic ordering was supressed in a thin surface layer, where the crystal order is supressed by defects. The ratio of the surface layer thickness to particle radius increased as the particle size decreased. This resulted in a relatively large proportion of magnetically and crystallographically disordered volume, when compared to the bulk samples [31]. Therefore, M_S became smaller than for the bulk crystal. Small H_C values were obtained for the nanoparticulate material, because the magnetic moment of each nanocrystallite making up this material was small enough to become perturbed by thermal excitation. There are no magnetic domains in such small nanocrystallites. An applied magnetic field easily rotates the magnetic moments and irreversibility effects and H_C occur because of weak interaction between neighbouring nanocrystallites.

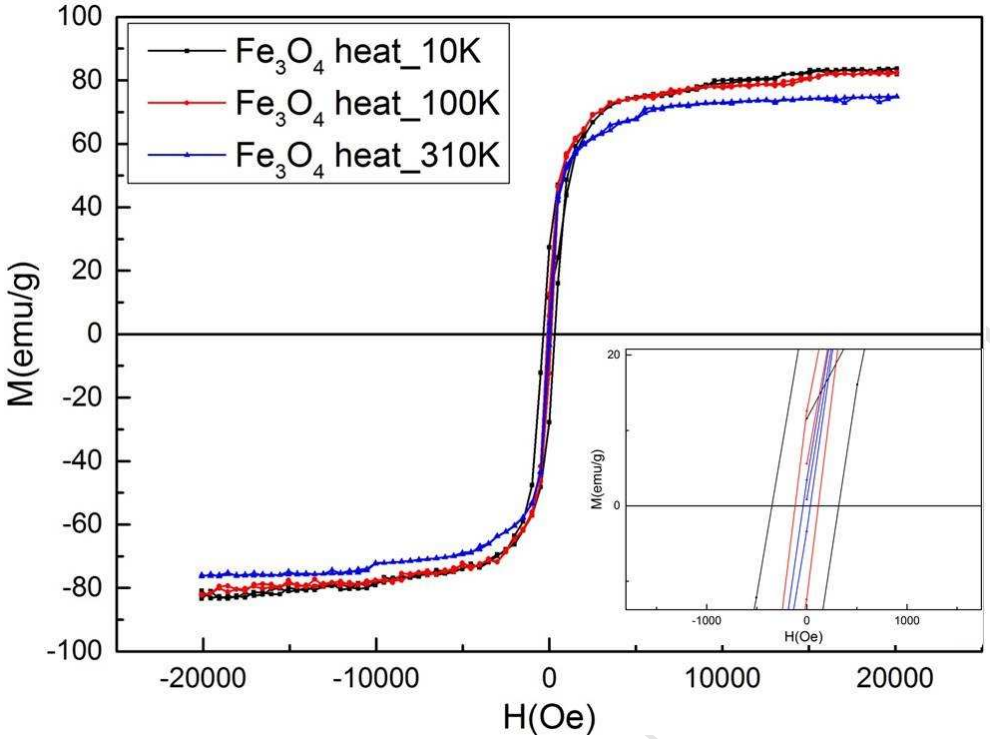

Figure 8.: The magnetic hysteresis loops of porous Fe_3O_4 at temperatures of 10, 100, and 310K. The zoomed low-field region (inset) shows values of the coercive field.

3.5 FT-IR measurements:

Most of the vibrations observed in Figure 6 are attributed to the bonds in aromatic rings related to methyl blue. According to the literature [32] aromatic hydrocarbons produce absorptions peaks in the regions 1600-1585 cm^{-1} and 1500-1400 cm^{-1}. This is in very good agreement with the peaks observed here at 1585 cm^{-1} (C–C stretch in-ring), and 1495 cm^{-1} (C–C stretch in-ring). On the other hand, bands related to S=O vibration were observed at 1325 cm^{-1} (asymmetric stretching), and at 1327 cm^{-1} (stretching). The bands in the region between 3415 and 3473 cm^{-1} were associated with the stretching vibrations of water molecules (O–H). It is clear from FT-IR analysis that methyl blue dye can be adsorbed on the surface of a Fe_3O_4 porous structure. A pure Fe_3O_4 sample without exposure to methyl blue showed only bands related to vapor water in region between 1000 to 1250 cm^{-1}, and for CO_2 at 2360 cm^{-1}. The strong absorption band just at the edge of the sensitivity window of

the spectrometer at ~590 cm^{-1} was the ν_1 vibrational mode of Fe-O[28,30], observed for all metal-oxide bonds (Fig. 6).

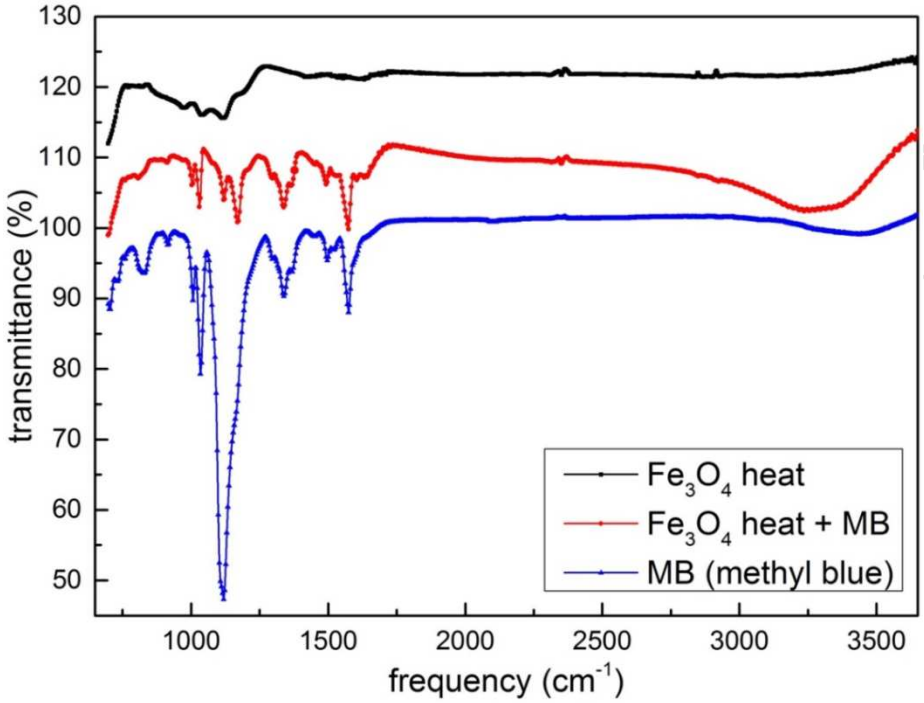

Figure 9.: FTIR spectra of as-prepared porous Fe_3O_4, porous Fe_3O_4 after exposure to methyl blue, and methyl blue.

3.6 UV-visible analysis:

Figure 7 shows the absorbance of light passing through a bottle containing water and porous Fe_3O_4 with adsorbed methyl blue, as a functions of time after application of a combined AC/DC magnetic fields (AC, f=10Hz), and a DC field only for periods between 1 and 60 minutes. Figure 8 shows the equivalent plot for an applied AC field only.

The intensity of the absorption peak at 580 nm increases with the time after which the AC/DC field, and AC fields only were applied, due to increased concentration of methyl blue released into the water. The effect of an AC/DC field (Figure 7) is greater than that of an AC field only (Figure 8), by a factor of about two. The release of methyl blue to the water as a function of magnetic field type and time is shown in Figure 9.

For the applied DC magnetic field only, no release of methyl blue was detected. With application of an AC field only, substantial absorbance due to methyl blue was detected even when the field was applied for just 1 minute. Longer exposure to an AC field resulted in an increased absorbance, although the rate of increase had begun to taper off at 60 mins. This effect was seen with magnetic field frequencies as low as 1 Hz (not shown), but higher frequencies resulted in a faster release of methyl blue. However, when both DC and AC magnetic fields were applied simultaneously the release of methyl blue was faster than with the AC field only (Figure. 7-9).

The response of the system to low frequency AC fields helped explain the mechanism of the release of methyl blue. Direct visual inspection of the magnetic nanopowder in the water showed that the application of an AC only field resulted in barely visible movement of the Fe_3O_4 nanopowder which settled at the bottom of the bottle.

However, application of a DC field using an Nd-B-Fe magnet near the bottle caused the Fe_3O_4 nanopowder to line up forming filaments at the bottom of bottle (Figs. 10c-e).

These filaments vibrated when an AC magnetic field was also applied. This movement of Fe_3O_4 nanostructures in water is responsible for the release of methyl blue.

Application of a DC field only did not stimulate release of MB, as the nanopowder did not move. The permanent magnetic field kept the dye enclosed in the magnetic material, disabling the usual vibrations of particles in the fluid (water) caused by the kinetics of molecules of water.

Importantly, the application of an AC field only resulted in a slow release of MB, affecting only small number of nanopowder in the area of separation line between the two poles, with much less obvious amplitude of oscillation (video 1). In contrast, when a combined AC/DC field was applied, particle alignment (agglomeration) in filaments induced by the DC field

greatly increased the particle oscillation, and release occurred uniformly in the whole area due to the effects of the AC field (videos 2, 3, 4).

As can be seen from our experimental data (Figure 9) the combined AC and DC magnetic fields released 40% more dye than with the AC field only, and a negligible amount of dye was released when the DC field of a permanent magnet was applied.

We attribute the release behaviour of this material to be a result of the friction between oscillating particles and fluid (water), and friction between the aligned particles. A DC field causes alignment of particles, but no vibration, and thus causes negligible release. A pure AC field causes particles to oscillate and frictional interactions with neighbouring particles, causes some release. However, the particles are not strongly bound together, and so these interactions are not strong and affect a limited number of particles. The application of a combined DC and AC field results in both strong alignment (bonding) and oscillations. This greatly increases the frictional interactions between the particles themselves and between particles and the fluid (water) as well, leading to the highest release rate of methyl blue.

To test how much of MB can be loaded into the porous Fe_3O_4, 2.35 mg of MB was diluted in 50 ml of deionised water. 8.23 mg of porous Fe_3O_4 was added into equivalent second solution. Both solutions were left standing for 24 hours. Measurements of the absorption coefficient in visible light for both solutions showed that 0.48 mg of MB was withdrawn from the water solution by porous Fe_3O_4. This implies that the Fe_3O_4 absorbed 6 wt% of MB.

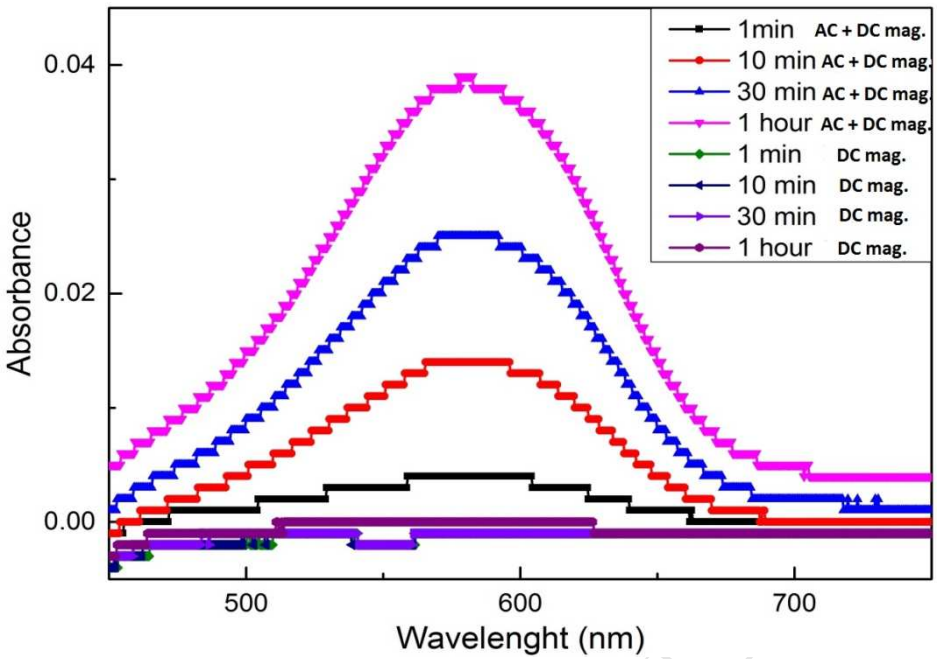

Figure 10.: Absorbance of light passing through water into which methyl blue is released from Fe_3O_4 nanostructures upon application of combined AC/DC magnetic fields (f=10Hz), and DC magnetic field only. The field was applied for periods of between 1 and 60 minutes.

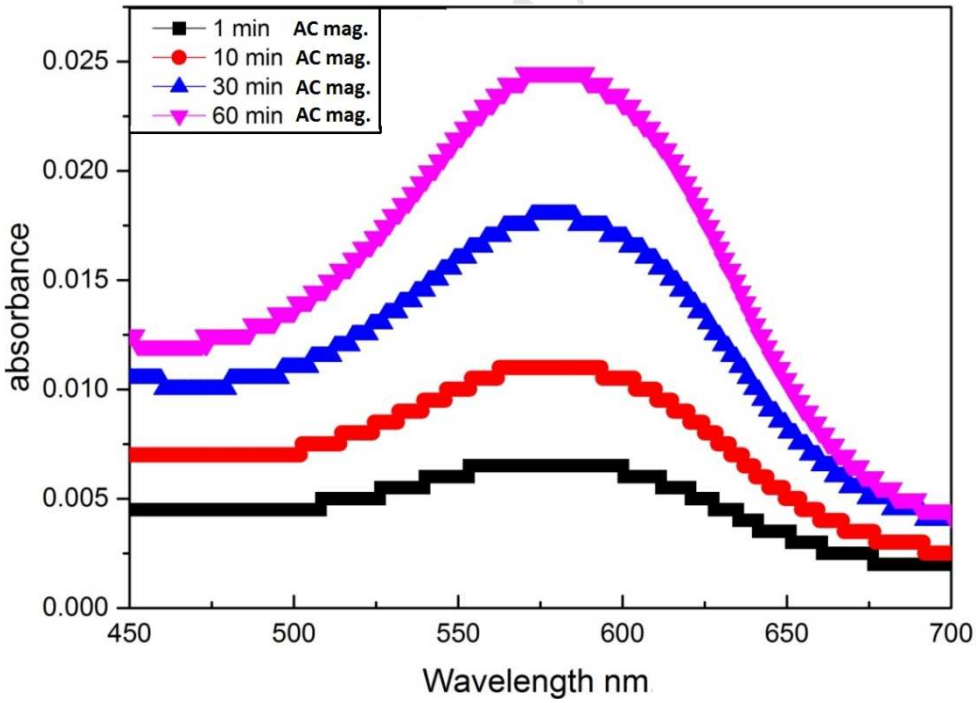

Figure 11.: Absorbance of light passing through water into which methyl blue is released from Fe_3O_4 nanostructures upon application of AC magnetic field (f=10Hz). The field was applied for periods between 1 and 60 minutes.

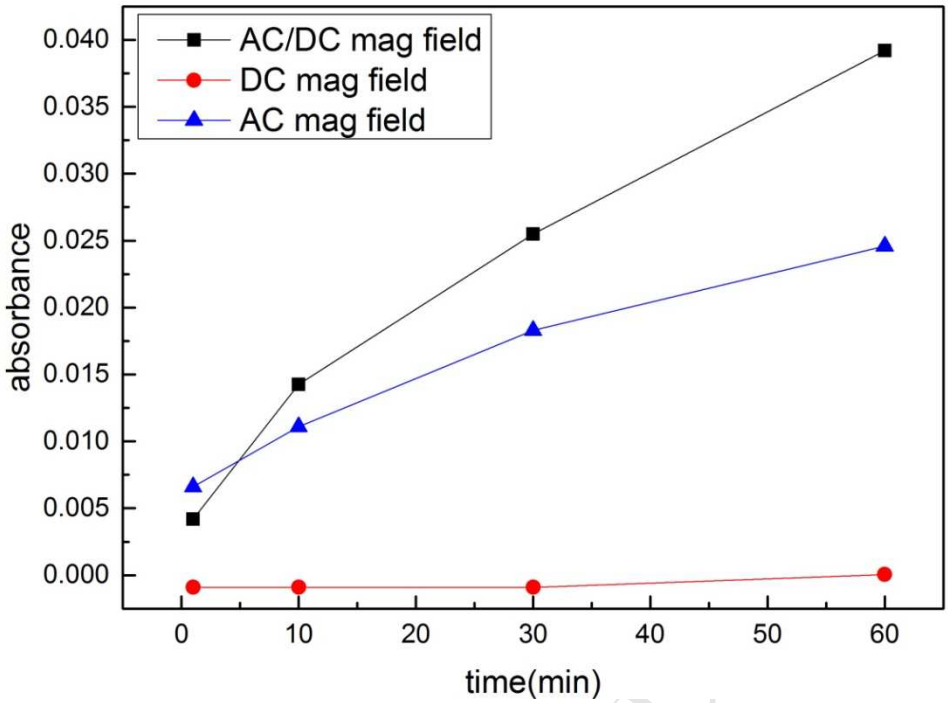

Figure 12.: Influence of magnetic field type on the release of MB as a function of time AC (blue triangles), combined AC/DC (black squares), and DC only (red circles). (AC fields are 10 Hz).

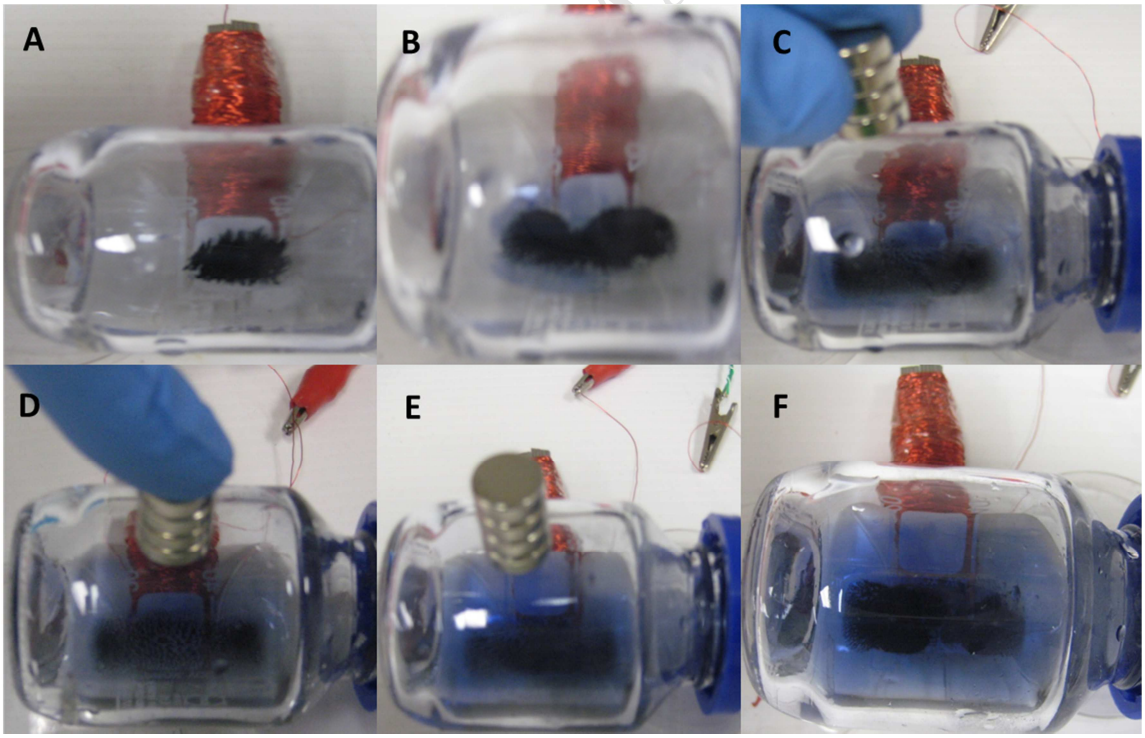

Figure 13. A photo of the hybrid magnets setup in time lapse. *a)* shows nanopowder before application of any magnetic fields; *b)* presents nanopowder for only AC applied; *c),d),e)* show nanopowder for applied both AC and DC magnetic fields.

4. Conclusions:

A simple candidate drug delivery system using porous Fe_3O_4 has been trialled. Methyl blue has been used as a surrogate drug, due to the convenience of monitoring its release photometrically. Fe_3O_4 is biocompatible, obviating the need for barrier coatings which might impact on the drug take-up and release performance. DC fields alone cause particle alignment, but no release. AC fields induced modest release. However, the greatest release occurred in the presence of a combined AC and DC field. We attribute the release process to be due to frictional interactions among particles by themselves, and particles and fluid (water), as they oscillate in an AC field. The enhanced release observed in a combined AC/DC field regime is due to increased interaction between oscillating particles as a result of alignment in the DC field. A list of potential advantages and disadvantages of this approach is given below.

Advantages of the AC/DC setup as a drug delivery system:

1) Simple set up, one permanent magnet, one AC magnet which can be readily aligned with various human body parts.
2) Maximal drug release induced by combined AC/DC field, enabling highly localised delivery.
3) Strong release performance even at very modest magnetic field strengths.
4) The drug delivery system is chemically simple and easy to synthesise and control.
5) Good biological compatibility of the delivery and release systems.
6) Considerable potential for chemical and structural refinement to improve performance.

Disadvantages of the DC/AC of the AC/DC setup as a drug delivery system:

1) Difficulties in removing porous material (particles) from the human body.
2) Precise release of drugs is challenging within the larger parts of human body such as the abdominal cavity, thorax, and skull.

Acknowledgments:

This work was supported by the 'AIIM (Australian Institute for Innovative Materials) for Gold/2014/2015 and University of Wollongong's Global Challenge Program/2015 grant in collaboration with Victor Chang Cardiac Research Institute.
This research the JEOL ARM200F microscope funded by the Australian Research Council (ARC) – Linkage, Infrastructure, Equipment and Facilities (LIEF) grant LE120100104 located at the UOW Electron Microscopy Centre
We also thank to the National Health and Medical Research Council for a Principal Research Fellowship to Prof. Boris Martinac.
Special thanks to Dr. Žižek and Prof. Matijević from University of Zagreb for porosimetry analysis and Prof. Yoon-Bo Shim from Pusan National University for cytotoxicity test.

References:

1. V.P. Torchilin, V.S. Trubetskoy, K.R. Whiteman, P. Caliceti, P. Ferruti, F.M. Veronese, New synthetic amphiphilic polymers for steric protection of liposomes in vivo, J. Pharm. Sci. 84 (1995) 1049-53.
2. V. Weissig, K.R. Whiteman, V.P. Torchilin, Accumulation of proteinloaded long-circulating micelles and liposomes in subcutaneous Lewis lung carcinoma in mice, Pharm. Res. 15 (1998) 1552-6.
3. P.K Working, M.S. Newman, T. Sullivan, J. Yarrington, Reduction of the cardiotoxicity of doxorubicin in rabbits and dogs by encapsulation in long-circulating, pegylated liposomes. J. Pharmacol Exp. Ther. 289 (1999) 1128 –33.
4. M. Jahanshahi, Z. Babaei, Protein nanoparticle: a unique system as drug delivery vehicles, Afr. J. Biotech. 7 (2008) 4926.
5. F. Yuan, Transvascular drug delivery in solid tumors. Semin. Radiat. Oncol., 8 (1998)164 –75.
6. J.F. Kukowska-Latallo, K.A. Candido, C. Zhengyi C, et al. Nanoparticle targeting of anticancer drug improves therapeutic response in animal model of human epithelial cancer. Cancer Res. 65 (2005) 5317–24.
7. U. Schroeder, P. Sommerfeld, S. Ulrich, B.A. Sabel, Nanoparticle technology for delivery of drugs across the blood–brain barrier, J. Pharm. Sci. 87 (1998) 1305–1307.
8. J. Kreuter, Nanoparticulate systems for brain delivery of drugs. Adv. Drug. Deliv. 47 (2001) 65–81.
9. O.C. Farokhzad, J. Cheng, B.A. Teply, et al. Targeted nanoparticleaptamer bioconjugates for cancer chemotherapy in vivo. Proc. Natl. Acad. Sci. USA 103 (2006) 6315–20.
10. H.S. Yoo, K.H. Lee, J.E. Oh, T.G. Park, In vitro and in vivo anti-tumor activities of nanoparticles based on doxorubicin–PLGA conjugates. J. Control. Release. 68 (2000) 419–31.
11. M. Yokoyama, M. Miyauchi, N. Yamada, T. Okano, Y. Sakurai, K. Kataoka, S. Inoue, Characterization and anticancer activity of the micelle-forming polymeric anticancer drug adriamycin-conjugated poly (ethylene glycol)-poly(aspartic acid) block copolymer. Cancer. Res. 50 (1990)1693-700.

12. J. Chatterjee, Y. Haik, C.J. Chen, Modification and characterization of polystyrene-based magnetic microspheres and comparison with albumin-based magnetic microspheres. J. Magn. Magn. Mater. 225 (2001) 21-9.
13. B. Bittner, B. Ronneberger, R. Zange, C. Volland, J.M. Anderson, T. Kissel, Bovine serum albumin loaded poly(lactide-co-glycolide) microspheres: the influence of polymer purity on particle characteristics, J. Microencapsul. 15 (1998) 495–514.
14. K. Paal, J. Muller, L. Hegedus, High affinity binding of paclitaxel to human serum albumin. Eur J Biochem. 268 (2001)2187–91.
15. D. Le Garrec, J. Taillefer, J.E. Van Lier, V. Lenaerts, J.C. Leroux, Optimizing pH-responsive polymeric micelles for drug delivery in a cancer photodynamic therapy model. J Drug. Target. 10 (2002) 429-37.
16. T. Wang, V.A. Petrenko, V.P. Torchilin. Paclitaxel-loaded polymeric micelles modified with MCF-7 cell-specific phage protein: enhanced binding to target cancer cells and increased cytotoxicity. Mol Pharm 2010.
17. H.S. Yoo, E.A. Lee, T.G. Park, Doxorubicin-conjugated biodegradable polymeric micelles having acid-cleavable linkages. J. Control. Release. 82 (2002)17-27.
18. H. Li, Z. Lu, G. Cheng, K. Rong, F. Chena, R. Chen, HEPES-involved hydrothermal synthesis of Fe_3O_4 nanoparticles and their biological application. RSC Adv. 5 (2015) 5059-5067.
19. M. Mustapić, D. Pajić, N. Novosel, E. Babić, K. Zadro, M. Cindrić, J. Horvat, Ž. Skoko, M. Bijelić, A. Shcherbakov, Synthesis, structural characterization and magnetic properties of iron boride nanoparticles with or without silicon dioxide coating, Croat. Chem. Acta 83 (2010) 275–282
20. A. Akbarzadeh, H. Mikaeili, N. Zarghami, R. Mohammad, A. Barkhordari, S. Davaran, Preparation and in vitro evaluation of doxorubicin-loaded Fe_3O_4 magnetic nanoparticles modified with biocompatible copolymers., Int. J. Nanomedicine. 7 (2012)511-26.
21. Y. Nakayama, M. Mustapić, H. Ebrahimian, P. Wagner, J.H. Kim, Md Sh. Al Hossain, J. Horvat, B. Martinac, Magnetic nanoparticles for “smart liposomes”, Eur. Biophys. J. (2015).
22. Z. Huang, F. Li, B.g Chena, G. Yuan, Nanoporous photocatalysts developed through heat-driven stacking of graphitic carbon nitride nanosheets, RSC Adv. 5 (2015) 14027-14033
23. S. Brunauer, P. H. Emmett, E. Teller, Adsorption of gases in multimolecular layers, J. Amer. Chem. Soc., 60, (1938) 309
24. E. P. Barrett, L. G. Joyner, P. P. Halenda, The determination of pore volume and area distributions in porous substances I computations from nitrogen isotherms, J. Am. Chem. Soc., 73, (1951) 373–380
25. M. Mustapić, J. Horvat, M. S. Hossain, Ž. Skoko and S. X. Dou, “Novel synthesis of superparamagnetic Ni-Co-B nanoparticles and their effect on superconductor properties of MgB_2”, Acta Mater. 70 (2014) 298–306.
26. M. Mustapić, J. Horvat, M. S. Hossain, Ž. Skoko and S. X. Dou, “Enhancing superconducting properties of MgB_2 pellets by addition of amorphous magnetic Ni-Co-B nanoparticles”, Supercond. Sci. Technol. 26 (2013) 075013.

27. H.El Ghandoor, H. M. Zidan, Mostafa M.H. Khalil and M. I. M. Ismail, Synthesis and some physical properties of magnetite (Fe_3O_4) nanoparticles, Int. J. Electrochem. Sci., 7 (2012) 5734 – 5745
28. L.-H. Shen J.-F. Bao, D. Wang, Y.-X. Wang, Z.-W. Chen, L. Ren, X. Zhou, X.-B. Ke, M. Chena, A.-Q. Yanga, One-step synthesis of monodisperse, water-soluble ultra-small Fe_3O_4 nanoparticles for potential bioapplication, Nanoscale, 5 (2013) 2133.
29. P.L. Hariani, M. Faizal, R. Marsi, D. Setiabudidaya, Synthesis and properties of Fe_3O_4 nanoparticles by co-precipitation method to removal procion dye, International Journal of Environmental Science and Development, 4 (2013) 3.
30. J. Sun, S. Zhou, P. Hou, Y. Yang, J. Weng, X. Li, M. Li, Synthesis and characterization of biocompatible Fe_3O_4 nanoparticles, Journal of Biomedical Materials Research Part A, DOI 10.1002/jbm.a
31. W. Wu, Q. He, C. Jiang, Magnetic iron oxide nanoparticles: synthesis and surface functionalization, Nanoscale Res. Lett. 3 (2008) 397–415
32. Aldrich Library of Infrared Spectra, 3rd Ed. C. Pouchert, Aldrich Chemical Co., 1981, 1850 pp.

Highlight

1) We present simple set up for efficient drug delivery
2) Maximal drug release induced by combined AC/DC field, enabling highly localised delivery.
3) Strong release performance even at very modest magnetic field strengths.
4) The drug carriers (Fe_3O_4) are chemically simple and easy to synthesise and control.
5) Good biological compatibility of the delivery and release systems.